Towards the numerical simulation of 5 Floating Point Absorber Wave Energy Converters installed in a line array using OpenFOAM

Brecht Devolder[#*1], Pieter Rauwoens[*2], Peter Troch[#3]

[#]*Department of Civil Engineering, Ghent University*
Technologiepark 904, 9052 Ghent, Belgium

[1]Brecht.Devolder@UGent.be

[3]Peter.Troch@UGent.be

[*]*Department of Civil Engineering, Technology Cluster Construction, KU Leuven*
Zeedijk 101, 8400 Ostend, Belgium

[2]pieter.rauwoens@kuleuven.be

***Abstract*— In this paper we use the CFD toolbox OpenFOAM to perform numerical simulations of multiple floating point absorber Wave Energy Converters (WECs) in a numerical wave basin. The two-phase Navier-Stokes fluid solver is coupled with a motion solver to simulate the wave-induced rigid body heave motion. The purpose of this paper is twofold. The first objective is to extend numerical simulations of a single WEC unit to multiple WECs and to tackle the issues of modelling individual floating objects close to each other in an array layout. The second objective aims to include all the physical processes (e.g. friction forces) observed during experimental model tests in the numerical simulations. The achievements are verified by validating the numerical model with laboratory experiments for free decay and regular wave tests using a line array of two and five WECs. For all the simulations presented, a good agreement is found between the numerical and experimental results for the WECs' heave motions, the surge forces on the WECs and the perturbed wave field. As a result, our coupled CFD–motion solver proves to be a suitable and accurate toolbox for the study of wave-structure interaction problems of WEC arrays.**

***Keywords*— Wave energy, floating point absorber, array, coupled CFD–motion solver, verification and experimental validation.**

I. Introduction

Wave energy from ocean waves is captured by Wave Energy Converters (WECs) and converted into electrical power. In this study, WECs of the floating point absorber (FPA) type are selected. In order to extract a considerable amount of wave power at a location in a cost-effective way, a large number of WECs are arranged in arrays using a particular geometrical configuration. Firstly, interactions between the individual WECs (near field effects) affect the overall power production of the array. One should avoid, for instance, that one WEC is positioned in the wake region of another WEC within the array for a specific sea state. Secondly, the wave height reduction behind one or more WEC arrays (far field effects) affects other users in the sea, the environment or even the coastline. By using a numerical model, supported by experimental validation data, we aim to develop a methodology (and a related numerical tool) to answer the fundamental underlying questions on WEC array design: finding the optimal and cost-effective configurations of WEC arrays for power production, and quantifying the related environmental impact.

Pioneering research on WEC arrays has been carried out by Budal [1], Evans [2] and Falnes [3], which resulted in analytical expressions for the maximum power absorption of arrays. Due to the limited computational power at that time, the derivations are restricted to a linear theory. In the past decades, the computational power has been increased significantly, enabling the use of complex models for WEC array modelling. In this research, the Computational Fluid Dynamics (CFD) toolbox OpenFOAM [4] is used to study array effects in a numerical wave basin by solving the three dimensional flow field around the WECs and their response. Moreover, CFD is able to include viscous, turbulent and non-linear effects which may be absent in simplified radiation-diffraction models such as linear potential flow solvers based on boundary element methods. The numerically obtained viscous flow field around and the response of a single WEC unit have been verified and validated with experimental data in previous work of the authors [5]. Now, the main focus of this paper is to demonstrate the ability of our coupled CFD–motion solver to simulate multiple independently moving WECs arranged in different array configurations subjected to regular waves. In particular, the hydrodynamics around and the response of respectively two and five WECs installed in a line are studied. Only the heave motion of the WECs is considered and together with the surge force on the WECs and the perturbed wave field verified and validated with experimental results.

The capability of OpenFOAM to study wave-body interactions is already illustrated in [6]. An excellent description and comparison of the different numerical models for wave energy devices is provided in [7]. They mentioned that good agreements have been obtained between CFD and experimental results, demonstrating the feasibility of CFD simulations for wave energy applications. As mentioned

before, CFD simulations of a single WEC unit have been reported in previous work of the authors [5] but also in [8], [9]. Numerical simulations of WEC arrays using simplified radiation-diffraction models have been published in [10]–[12]. However, CFD simulations of a WEC array have only been reported by a few researchers, e.g. [13], [14]. In [13], only a brief introduction regarding an array of two WECs subjected to regular waves is reported. It is also mentioned that more simulations are needed in order to fully quantify the interactions between multiple WECs. More recently, [14] performed free decay tests of different WEC arrays. However, simulations regarding the response of an array in a wave field are still lacking. Very recently, we published in [15] the first results using our coupled CFD–motion solver for simulating free decay tests (2WEC and 5WEC-array) and a regular wave test (2WEC-array). In the present paper, improvements are made hereto. Moreover, the focus in [15] was put on the numerical simulation of free decay tests without power take-off (PTO) system rather than WECs, for which the PTO system was activated, subjected to regular waves. Therefore in this paper, numerical simulations are performed for a free decay test and regular waves using WECs (including a PTO system) arranged in a small array.

II. Experimental Setup

In this study, experimental data are used from the WECwakes project [16] conducted in the shallow water wave basin of the Danish Hydraulics Institute (DHI; Hørsholm, Denmark). The DHI wave basin has a length of 25 m, a width of 35 m and a height of 0.8 m. A constant water depth of 0.70 m was maintained during all the tests. Waves are generated by forty-four piston type wave paddles installed at one end of the DHI wave basin. One individual paddle segment is 1.2 m high and 0.5 m wide, resulting in a total width of the wave maker equal to 22 m. Moreover, each paddle segment is equipped with DHI AWACS (Active Wave Absorption Control System) to allow full control over the incident wave field. Each paddle segment has two wave gauges measuring the actual surface elevations. The average of these two surface elevations is used to control each paddle individually to obtain the target surface elevation at the paddle segment. This procedure will avoid reflection against the wave maker of the reflected and radiated waves within a certain frequency range. At the opposite end of the DHI wave basin, waves are absorbed by a stone gravel beach with a slope of approximately 1/5.59.

Up to 25 WEC units have been installed in the DHI wave basin using different geometric configurations. The geometry of an individual WEC unit is depicted in Fig. 1. The WECs are characterised by a mass m of 20.545 kg, a total height h_{WEC} of 0.60 m, a diameter D of 0.315 m and a draft d_{WEC} of 0.315 m. A supporting steel axis of 4 cm by 4 cm with a gravity metal base is installed through the WEC to simulate the heave motion only. Therefore, a square shaft bearing of 4.45 cm by 4.45 cm is present inside the WEC. Friction between the steel shaft and the WEC is limited by using PTFE bearings at the top and at the bottom. The presence of the supporting axis through each WEC unit is responsible for additional friction forces on the WEC. Those friction forces will remove energy from the system and increase the damping on the WEC's motion. The first contribution is caused by the viscous flow of water in between the shaft bearing and steel axis. Secondly, the wave induced horizontal force acting on the WEC will push the WEC's bearings against the supporting axis, generating sliding friction on the WEC. At the top of the WEC, the power-take off (PTO) system is installed (see Fig. 1) in order to extract energy from the incident wave field. The PTO force is applied to the WEC by mimicking a Coulomb damper using friction brakes (composed of two PTFE blocks and four springs) between the float and the supporting axis. Consequently, this PTO system is a third but the main contribution to the total friction force acting on the WEC in order to remove energy from the system and increase the damping on the WEC's motion.

In total, 23 different configurations of the WEC units have been installed in the DHI wave basin for various tests: free decay tests, fixed WECs (only diffraction), regular and irregular sea states. The wave field is recorded by 41 resistive wave gauges in order to measure the incident wave field, the perturbed wave field around the WECs and the wave field modification in the wake behind the array. Moreover, a potentiometer is attached to each WEC unit to measure its heave displacement. Additionally, two load cells are installed on the vertical supporting axis of five WEC units for measuring the surge force on those five WECs. As a result, an enormous experimental database is available which is of large interest for the validation and extension of different numerical models. In this paper, our coupled CFD–motion solver is validated by using the available experimental dataset generated during the WECwakes project.

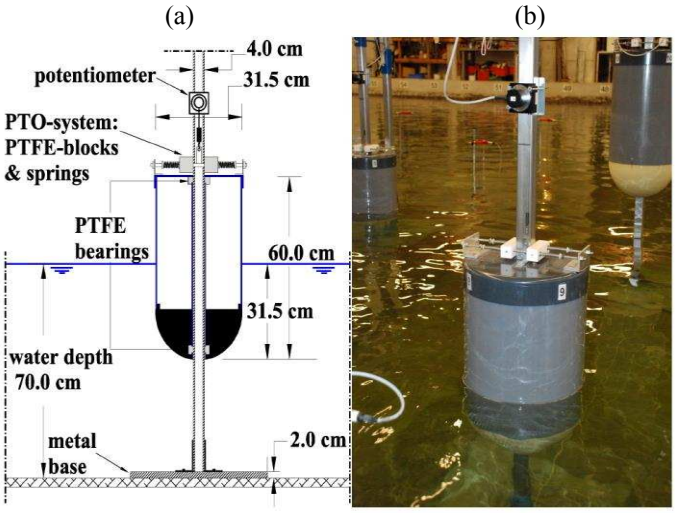

Fig. 1 (a) Definition sketch of the cross section of a WEC unit; (b) photograph of a WEC unit within an array installed in the DHI wave basin during the WECwakes project. Adopted from [16].

III. Numerical Framework

Numerical modelling is performed for the study of multiple individual WEC units configured in an array layout. The two-

phase flow solver with dynamic mesh handling, interDyMFoam, coupled to a rigid body motion solver is available in OpenFOAM [4]. It is used to perform numerical simulations of floating rigid bodies installed in a numerical wave basin.

A. Flow Solver

Simulations of the two-phase flow field are performed by solving the incompressible Reynolds-Averaged Navier-Stokes (RANS) equations, with a conservation equation for the Volume of Fluid (VoF) [17]. Turbulent effects are not dominating since the flow of the simulations presented is always characterised by a low Keulegan-Carpenter (KC) number. Therefore in the first instance, only laminar solutions are calculated. However, in case turbulence plays a major role (e.g. during flow separation or wave breaking events), we refer to [18] on how to properly deal with turbulence near the air-water interface. In that case, a buoyancy-modified *k-ω SST* turbulence model will be applied. That turbulence model results in a stable wave propagation model without significant wave damping over the length of the basin due to RANS turbulence modelling and it will also predict the turbulence level in the flow field more accurately at the locations where wave breaking occurs. As shown later on, the main features of the WEC's motion, surge forces on the WECs and the perturbed wave field are already captured by predicting a laminar solution only.

For all simulations the following discretisation schemes and solver settings are used: central discretisation for the pressure gradient and the diffusion terms; TVD (total variation diminishing) schemes with a van Leer limiter [19] for the divergence operators; second order, bounded, implicit time discretisation; a maximum Courant number of 0.30.

B. Computational Domain

All the numerical simulations are performed in a numerical wave basin which represents the experimental DHI wave basin as good as possible. As a simplification, one symmetry plane is used in order to obtain reasonable simulation times. The vertical symmetry plane goes through the centre of the WECs installed in the middle column (WEC1 to WEC5) and is implemented over the length of the basin, as indicated in Fig. 2. This is justified because no asymmetric effects are expected for the WEC configurations tested in this paper (low KC numbers).

We use the IHFOAM toolbox [20], [21] to implement the wave maker and absorbing beach in the experimental facility indicated as inlet and outlet respectively (see Fig. 2). The fully reflective side wall of the numerical wave basin is sufficiently far enough from the array, 5.7 m (decay test) and 11 m (regular waves test, see Fig. 2), to neglect its influence on the hydrodynamics around the WECs.

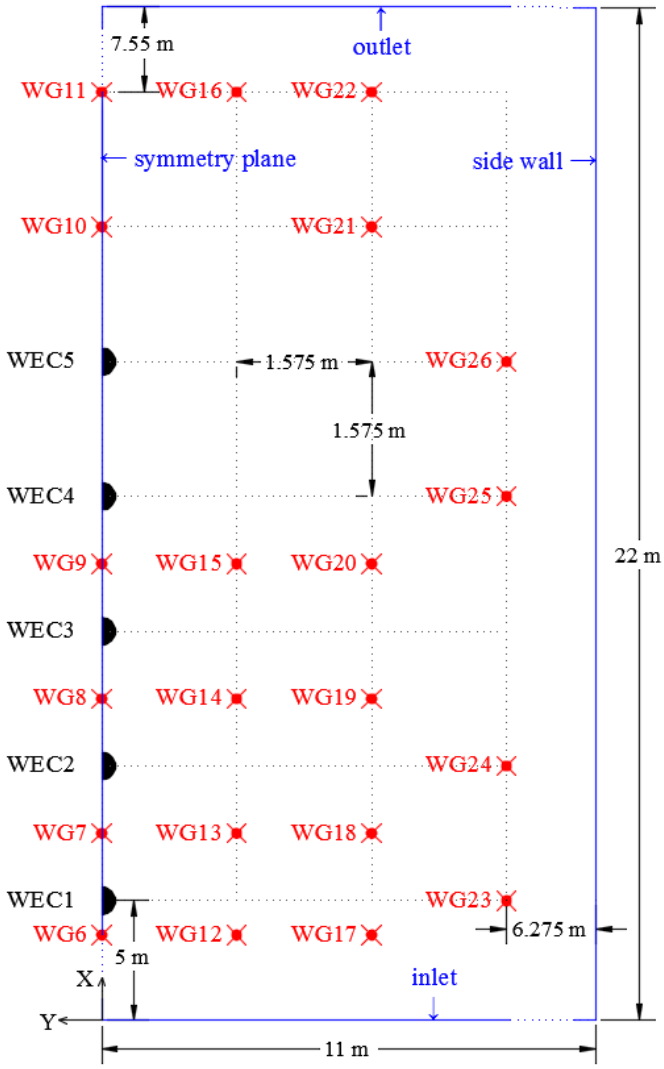

Fig. 2 Plan view (*XY*-plane) of the numerical wave basin using one symmetry plane on the left side and including all the WECs considered for the simulations presented. The red marks indicate the position of all the available wave gauges installed in the DHI wave basin.

The numerical wave basin is represented by a structured grid consisting of only hexahedral cells with local refinements in the zones of interest (i.e. around the free water surface and

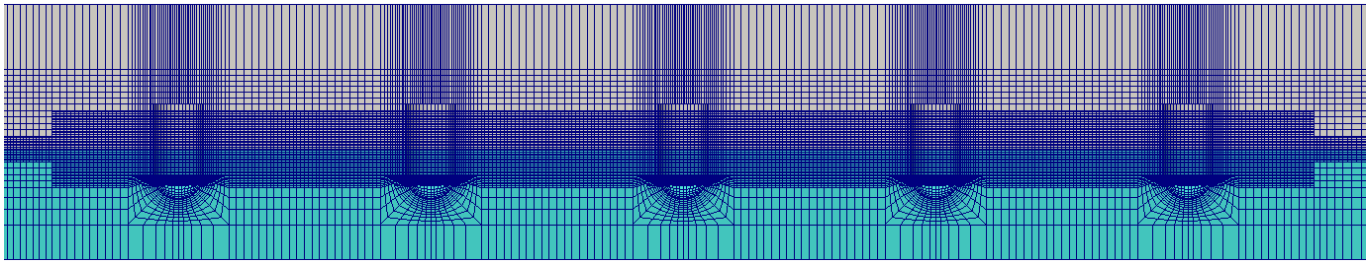

Fig. 3 Cross section (*XZ*-plane) of the computational domain for the 5WEC-array (WEC1 on the left to WEC5 on the right) (blue = water, grey = air).

around the WEC units). A longitudinal cross section of the numerical domain around the WECs is depicted in Fig. 3 for the 5WEC-array. The vertical grid resolution is about 1 cm in the zones of interest, which is sufficiently according to [5]. The horizontal cell size increases towards the boundaries of the numerical wave basin in order to limit the number of cells. The only exception is that the horizontal cell size is kept constant towards the inlet boundary in order to properly simulate wave propagation towards the WEC-array. The high aspect ratio observed for the cells above and beneath the WECs is explained in the next paragraph. In order to compare experimental and numerical results, an identical WEC geometry is needed. Because of the complexity of meshing the shaft bearing inside the WEC, another methodology is followed as reported in [5]. As a result, a grid around the WEC without that vertical shaft is obtained as shown in Fig. 3.

C. Rigid Body Motion

The CFD-fluid solver is coupled with a motion solver in order to simulate rigid body motions. Only the governing motion of the WEC's behaviour is considered, the heave motion. This assumption allows a reduction from a six to a one degree of freedom motion. During each time step in the transient simulation, an iterative procedure is needed to obtain a converged solution for both the fluid solver and the motion solver. We developed a method that accelerates this coupling procedure and hence reduces the amount of sub-iterations for each time step to a maximum of four. The key ingredient of this method is a good estimator for the WEC's hydrodynamic added mass, as discovered in [22].

A second order accurate Crank-Nicolson integration scheme is used to derive the position of the WEC from its acceleration a. The acceleration itself is based on Newton's second law: $F = ma$ in which the force F is the sum of the pressure, shear and gravity forces acting on all the boundary faces of the WEC calculated with the fluid solver minus the PTO force and friction forces caused by the supporting axis (see further in section IV). The WEC's mass m is determined using the procedure developed in [5] to account for the WEC's shaft bearing.

In order to simulate multiple independently moving WECs in an array configuration, arbitrary mesh interfaces (AMIs) are implemented in order to create sliding meshes (see dashed vertical lines in Fig. 4 for the case of two WEC units). These AMIs define a zone of cells around each WEC unit. In each zone, only the lowest and highest row of cells (see blue shaded boxes in Fig. 4) are expanded or compressed according to the motion of the WEC unit located in that zone. This is implemented to prevent undesirable mesh deformation (i.e. high non-orthogonality and skewness of the grid cells) around the air-water interface, reducing the discretisation error for the applied finite volume method. As a consequence, high aspect ratios are obtained for the distorted cells at specific time instants. However, those cells are not inside the zones of interest and will therefore not affect the accuracy of the simulations. All the variables solved with the flow solver, such as velocity, pressure and volume fraction, are interpolated over the AMIs.

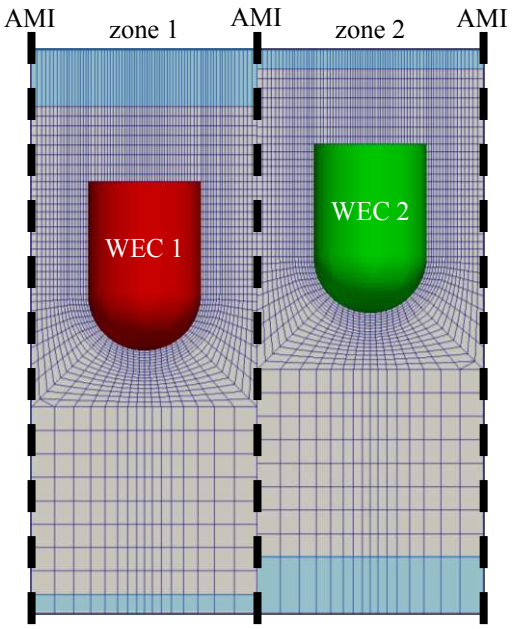

Fig. 4 A definition sketch of two independently moving WECs inside a three-dimensional computational domain of hexahedral cells. Only the highest and lowest row of cells (blue shaded boxes) in a zone are distorted (expanded or compressed) according to the heave motion of the WEC located in that zone. In between the zones, AMIs are implemented to create sliding meshes (dashed lines).

D. Free surface

The free surface between water and air is obtained by the Volume of Fluid (VoF) method [17]. The method is based on a volume fraction α which is 0 for a completely dry cell and 1 for a completely wet cell and in between 0 and 1 for an interface cell containing both water and air. In a post processing step, the position of the free water surface is determined by a discrete integration of the volume fraction α over a vertical line (Z-direction) divided in n equal parts:

$$z_{water\ level} = \sum_{i=0}^{n-1} \alpha_i (z_{i+1} - z_i)$$

IV. Results and Discussion

A complete overview of our available benchmark data, with both numerical and experimental results, is summarised in Table 1. In this paper, only the underlined tests and results as outlined in Table 1 are reported. Firstly, a free decay test is performed using a 2WEC-array of which the PTO system is activated. The free decay test is initialised by pushing one WEC down, release it instantaneously and monitor the response of the WEC itself, and the neighbouring WEC. Secondly, regular waves are generated to obtain the response of a 2WEC and 5WEC-array, the surge force acting on the individual WEC units and the resulting perturbed wave field.

TABLE I
A COMPLETE OVERVIEW OF THE AVAILABLE BENCHMARK DATA (NUMERICAL AND EXPERIMENTAL RESULTS).

Layout	Type of tests	Available results
2WEC-array → • •	Free decay (no PTO) Free decay (PTO) Regular waves (PTO)	WECs' heave motion Surge force on WECs Surface elevations
5WEC-array → • • • • •	Free decay (no PTO) Regular waves (PTO)	WECs' heave motion Surge force on WECs Surface elevations
9WEC-array → • • • • • • • • •	Regular waves (PTO)	WECs' heave motion Surge force on WECs Surface elevations

A. Free decay test using an array of 2 WECs (including PTO)

During this first test using a 2WEC-array, WEC5 is lifted higher than its equilibrium position, released, and a free decay test is started. At a distance of $5D$ = 1.575 m, WEC4 is freely floating in the water and will heave due to the radiated waves generated by WEC5. On both WECs the PTO system is activated. The aim of this free decay simulation is to correctly include all the friction forces in the numerical model due to the PTO system and the presence of the supporting axis through the WEC unit in the experimental model tests.

In a preliminary simulation, the influence of the supporting axis on the friction force acting on the WEC is neglected. Therefore, only one coulomb damper is included on each WEC because the PTO system was on during the experimental test. The PTO force is implemented in the numerical model according to Coulomb's friction law, as described in [16]:

$$F_{PTO} = -\mu F_{spring} sign(v(t)) = -\mu 4 dx k_{spring} sign(v(t))$$

where $v(t)$ is the WEC's vertical velocity, the coefficient of friction between PTFE and steel μ = 0.17, the spring compression increment dx = 30.5 mm and the spring stiffness coefficient k_{spring} = 0.14 N/mm. The numerically obtained heave motion of WEC5 as a function of time is shown in Fig. 5 using a black dashed line. It is clearly observed that the amplitude of that heave motion is larger than the experimental result, shown in red. In order to tune the numerical decaying motion to the experimental data to take the influence (i.e. viscous water flow) of the supporting axis into account, the methodology as reported in [5] is applied. As a result, a linear damper is needed returning an additional friction force on the WEC:

$$F_{LD} = -cv(t)$$

with a damping coefficient c equal to 4.86 kg/s for WEC5. For WEC4, the same damping coefficient is used. Since the excitation force on WEC4 due to the decaying motion of WEC5 is small and the PTO system is on, no heave motion is expected for WEC4. Remarkably, the value of the damping coefficient has been increased with a factor 2.6 compared to the value reported in [15] for the 2WEC-array without the PTO system activated. This means that the experimental PTO system cannot be modelled numerically by a coulomb damper only but also an additional linear damper is needed.

Subsequently, numerical simulations are performed by using both the PTO damper and the linear damper for two grid densities. The first grid has a vertical cell size of 0.01 m in the zones of interest, as previously mentioned. The second grid is based on the first grid in which all the cells are refined in all directions resulting in a vertical cell size of 0.005 m in the zones of interest. The resulting heave motion for WEC5 (decaying) is presented in Fig. 5 for the experimental data in red and the two numerical simulations in blue and green. Firstly as a verification of the numerical model, the two numerically obtained heave motions are extremely close to each other, only 2.5 % difference in amplitude is observed. Secondly, the numerical obtained decaying motion of WEC5 is validated with the experimental data, as shown in Fig. 5. However, some very small discrepancies are observed due to damping nonlinearities present during the experiments. It is however difficult to measure experimentally small heave motions due to friction of the bearings along the steel shaft (cf. the WECwakes experiments). For WEC4, there is no heave motion observed in both numerical and experimental results.

Additionally, the surge (horizontal) force on WEC4 due to the radiated wave field is compared between the numerical and experimental model and depicted in Fig. 6. Again, a good comparison is found during the verification and validation study. It is important to note that we filtered out the noise in the time signals of the experimental force measurements using a bandpass filter.

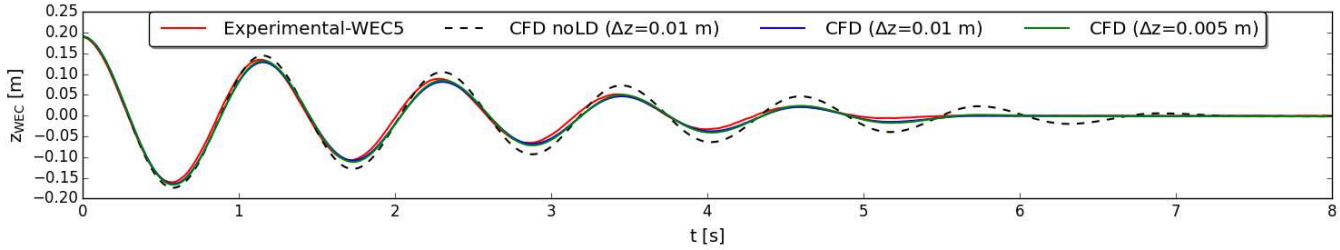

Fig. 5 Vertical position of WEC5 during a free decay test of WEC5 with respect to its equilibrium position (z_{WEC} = 0 m) obtained with CFD (dashed black, blue and green line) compared to experimental data (red line).

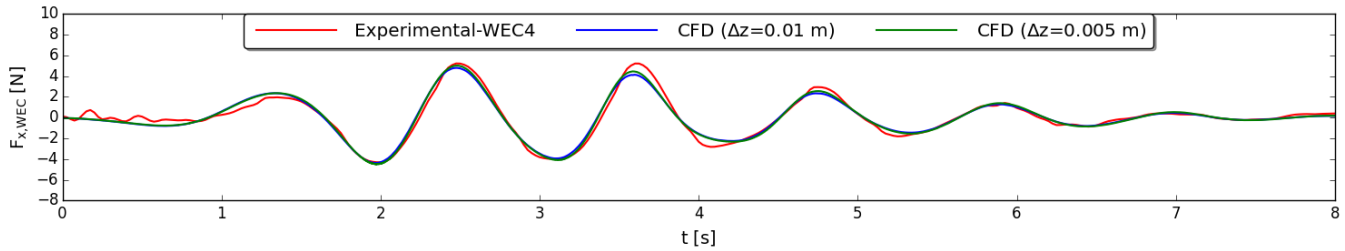

Fig. 6 Surge force acting on WEC4 during a free decay test of WEC5 obtained with CFD (blue and green lines) compared to the experimental determined surge force using two load cells after filtering the noise (red line).

Finally, the radiated wave field is given in Fig. 7 for both numerical and experimental data using WG9, WG10 and WG11 shown in Fig. 2. The maximum observed amplitude of these radiated waves is smaller than 1 cm. Despite these small-amplitude waves, all the results are very similar. In the first 6 seconds of the signals, the amplitude as well the phase of the radiated wave field is modelled close to the experimental results. Thereafter, some deviations between both results are observed due to the different behaviour of the numerical and experimental boundary conditions responsible for the absorption of the radiated waves. Subsequently, Fig. 8 visualises a snapshot of the radiated wave field generated by the decaying motion of WEC5 at t = 4.20 s. Around WEC4, a slightly modified radiated wave pattern is observed due to diffraction. As reported before, WEC4 is not moving and thus not generating radiated waves.

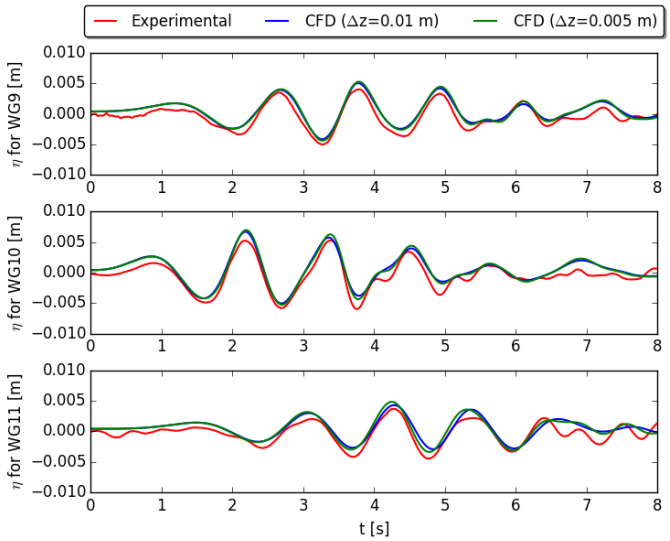

Fig. 7 Radiated wave field using several wave gauges (see Fig. 2) around the 2WEC-array during a free decay test of WEC5 obtained with CFD (blue and green lines) compared to the experimental measurements (red line).

As a conclusion based on the free decay test, the verification study justifies that a vertical cell size of 0.01 m in the zones of interest is sufficient to capture the main effects of the decaying motion of WEC5, the surge force on WEC4 and the radiated wave field. Moreover, the validation study proves that the use of both a coulomb damper and a linear damper is sufficient to include the main contributions of all the friction forces acting on the WECs in case no incident wave field is present.

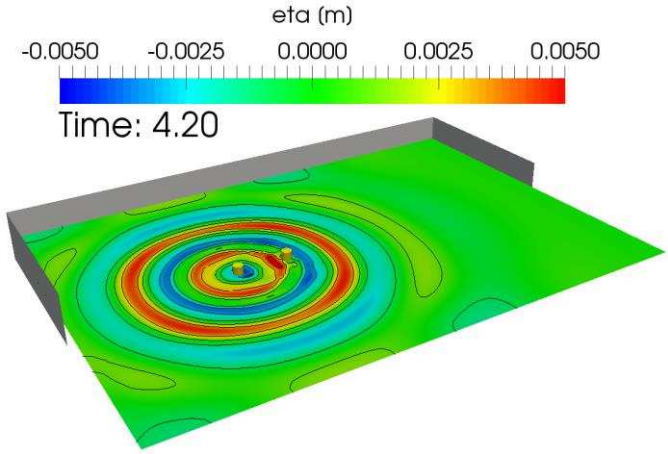

Fig. 8 A three dimensional snapshot of the radiated wave field around the 2WEC-array during a free decay test of WEC5 (left WEC) obtained with CFD.

B. Regular waves using an array of 2 WECs

The second simulation uses the same 2WEC-array, introduced in the previous section. This time, the two WECs are freely floating and regular waves are generated at the inlet. The waves have a height H equal to 0.074 m, a wave period T of 1.26 s and are generated in a water depth d of 0.70 m. At the inlet of the numerical wave basin, waves are generated using five paddle segments according to a second order Stokes theory and active wave absorption is turned on. On each WEC, two friction forces are applied as implemented for the free decay test (F_{PTO}, and F_{LD}) using the same values for the variables specified in the previous section. At this point, a similar numerical result will be obtained as reported in [15] with the only difference of the 2.6 times larger damping coefficient used for the linear damper. In [15], it is however concluded that the numerical obtained heave motions are significantly larger, about 60 %, than the experimental results. Moreover, there is also a time shift present in the signals for both WECs. Therefore, some improvements can be made as outlined in [15]. Firstly, the 2.6 times larger damping coefficient of the linear damper is applied. Those results are depicted using a dashed black line in Fig. 9 to Fig. 11. Secondly and in particular due to the presence of the incident wave field, a second coulomb damper is needed in order to take friction of the bearings on the supporting axis into account due to the wave induced horizontal force:

$$F_{bearings,X} = -\mu abs(F_{surge}(t))sign(v(t))$$

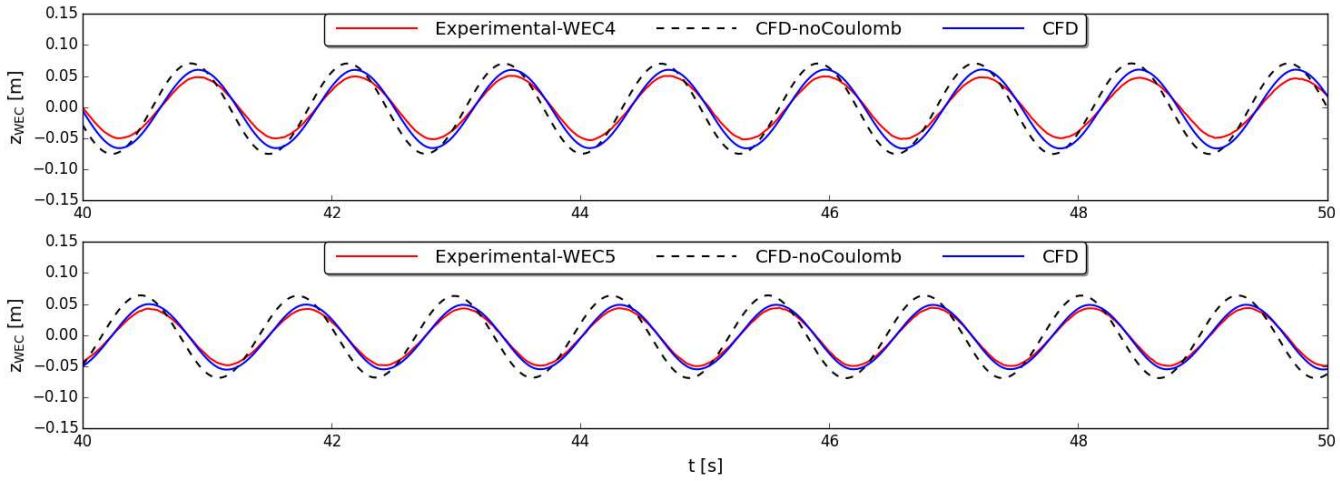

Fig. 9 Vertical position of WEC4 (top) and WEC5 (bottom) during a regular wave test (H = 0.074 m, T = 1.26 s, d = 0.70 m) obtained with CFD (dashed black and blue lines) compared to the experimental heave motions (red line).

where $v(t)$ is the WEC's vertical velocity, the coefficient of friction between PTFE and steel μ = 0.17 and $F_{surge}(t)$ the horizontal force in the X-direction acting on the WEC.

The heave motions of both WECs are visualised in Fig. 9 for the numerical and experimental model respectively. It is observed that the numerical obtained heave motions without the second coulomb damper are again 55 % larger than the experimental results (comparable to the 60 % reported in [15]). Those differences are reduced to 20 % if the second coulomb damper is included during the numerical simulations. Fig. 10 presents the surge force acting on both WECs. In contrast as observed for the heave motions, the numerical obtained surge forces are very similar to the experimental data. Moreover, there is no difference between the numerical simulations without and with the second coulomb damper. Lastly, the perturbed wave field (i.e. incident + diffracted + radiated wave field) is given in Fig. 11 for both numerical and experimental data using WG9, WG10 and WG11 (see Fig. 2). The time signals confirm that a similar wave field is present in the numerical wave basin as observed during the experimental tests. Again, the second coulomb damper is not influencing the perturbed wave field around the WECs. Fig. 12 depicts a snapshot of the perturbed wave field at t = 50 s. Waves are generated and absorbed at the right and left boundary respectively. The observed reduced wave height in the wake behind the 2WEC-array is due to the increasing aspect ratio of the grid cells. This increasing aspect ratio is responsible for numerical wave damping. This is however beneficial in order to avoid wave reflection from the absorbing outlet boundary. Around the array, a perturbed wave field is observed in the numerical wave tank. As a result, the radiated waves generated by each WEC are slightly influencing the numerically predicted heave motion of the other WEC. This is also illustrated in Fig. 9 by observing a different amplitude of the numerically obtained heave motions for both WECs, 0.07 m and 0.05 m for WEC4 and WEC5 respectively.

As a conclusion, only a different behaviour in the amplitude of the WECs' heave motions is observed between numerical and experimental data. Therefore, we assume that those discrepancies are mainly related to the unknown physical behaviour of the friction forces caused by the supporting axis in the experimental model.

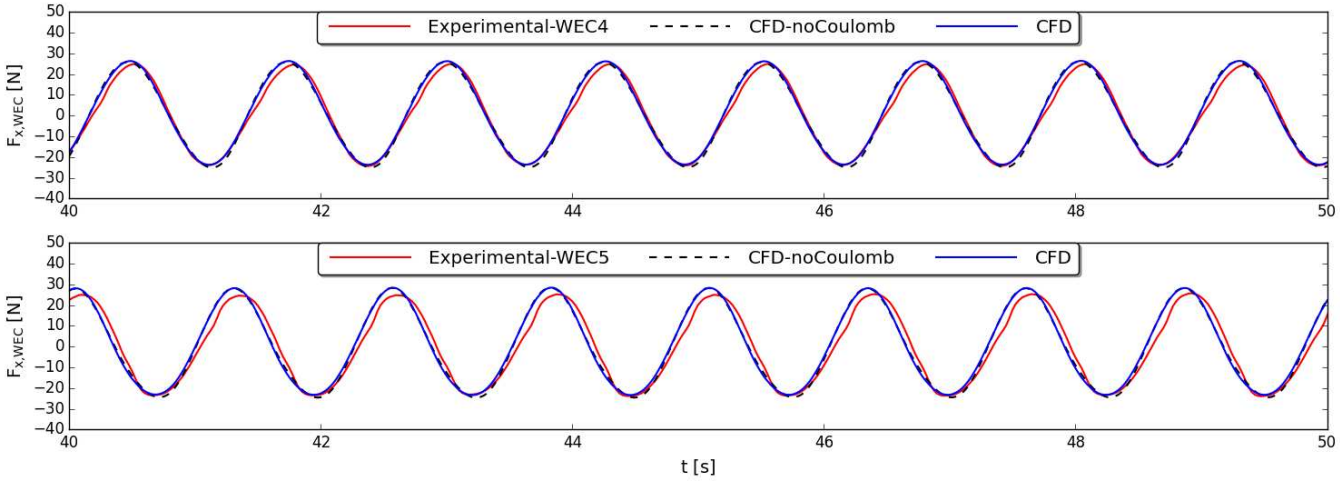

Fig. 10 Surge force acting on WEC4 (top) and WEC5 (bottom) during a regular wave test (H = 0.074 m, T = 1.26 s, d = 0.70 m) obtained with CFD (dashed black and blue lines) compared to the experimental measurements after filtering the noise (red line).

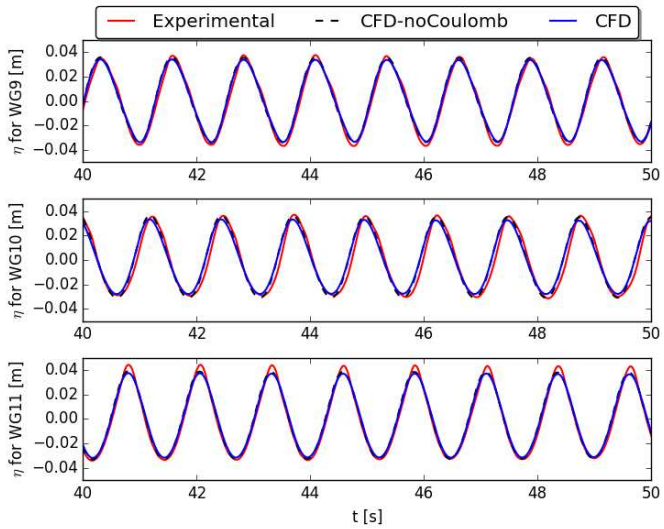

Fig. 11 Perturbed wave field using several wave gauges (see Fig. 2) around the 2WEC-array during a regular wave test (H = 0.074 m, T = 1.26 s, d = 0.70 m) obtained with CFD (dashed black and blue lines) compared to the experimental data (red line).

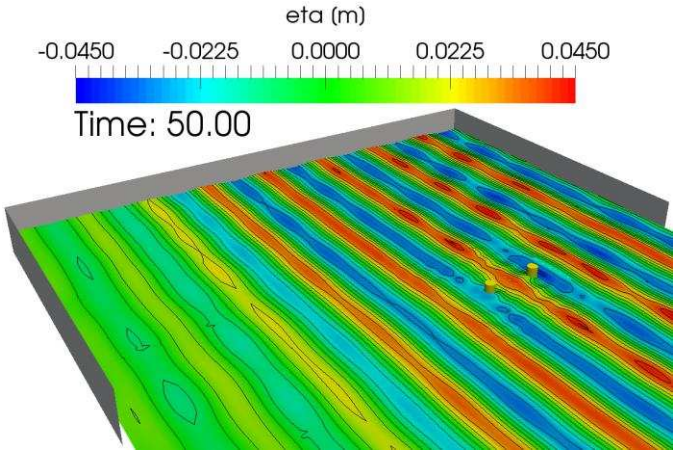

Fig. 12 A three dimensional snapshot of the perturbed wave field around the 2WEC-array during a regular wave test (H = 0.074 m, T = 1.26 s, d = 0.70 m) obtained with CFD.

C. Regular waves using an array of 5 WECs

Subsequently, three more WECs are added to the numerical wave basin resulting in an array of five WEC units installed in a line: WEC1 to WEC5 (see Fig. 2 and Fig. 3). On each WEC, additional friction forces (F_{PTO}, $F_{bearings,X}$ and F_{LD}) are applied with identical parameters as the regular wave test using the 2WEC-array, which has been reported in the previous section.

The heave motions of the five WECs as a function of time are given in Fig. 13 for both experimental and numerical data. The time series reveal that in general both results are comparable. However, significant differences in amplitudes are observed for WEC1 and WEC4. Remarkably for WEC2, the numerically predicted heave motion shows a phase difference with the experimental data. As concluded in the previous section, those differences are possibly related to incorrect or missing damping processes along the supporting axes through the WECs used for the experimental tests. For example, during the WECwakes experiment it is noticed that the friction characteristics change due to fouling of the supporting axes. Therefore before each testing day, the supporting axes were cleaned in order to minimise that particular model effect. A better validation of the numerical model is found when comparing numerical and experimental data for the perturbed wave field around the WECs (Fig. 14). The surface elevations around the WECs, are less influenced by the friction forces acting on the WEC due to the supporting axes. However, some discrepancies are observed regarding the time series of the surface elevations in the wave basin. Those differences between experimental and numerical data are possibly caused by model effects in the experimental setup and numerical errors in simulations presented. For example, it is reported in [16] that a spatial variation of the wave field is observed across the width of the experimental DHI wave basin when long-crested waves were generated. The difference in wave absorption between the experimental and the numerical wave basin is another possible cause to justify the observed discrepancies.

Fig. 15 depicts a snapshot of the perturbed wave field at t = 50 s. Similar to Fig. 12, waves are generated and absorbed at the right and left boundary respectively. Again, the reduced wave height in the wake behind the 5WEC-array is due to the increasing aspect ratio of the grid cells leading to numerical wave damping. Around the array, a significantly perturbed wave field is predicted by the numerical model. At particular locations, hotspots in surface elevations are observed due to the combination of the incident, diffracted and radiated wave fields. Moreover, the radiated waves generated by each WEC are influencing the numerically predicted heave motion of the other WEC (see also the blue lines in Fig. 13). Furthermore, an important reduction in wave height is observed in the wake behind the array.

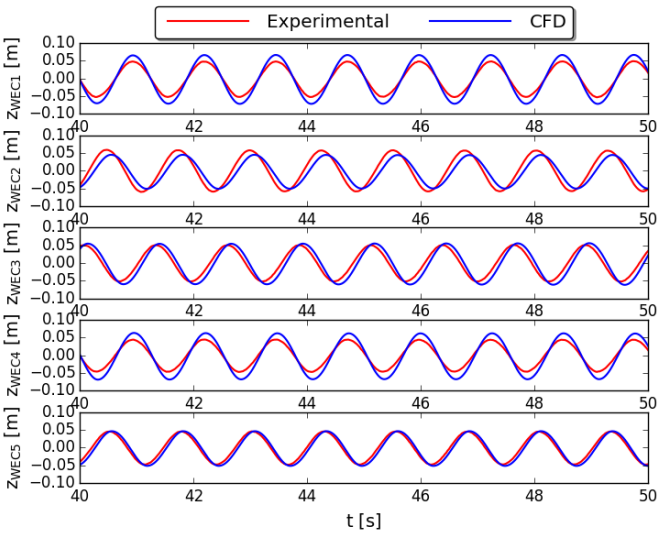

Fig. 13 Vertical position of WEC1 (top) to WEC5 (bottom) during a regular wave test (H = 0.074 m, T = 1.26 s, d = 0.70 m) obtained with CFD (blue line) compared to the experimental heave motions (red line).

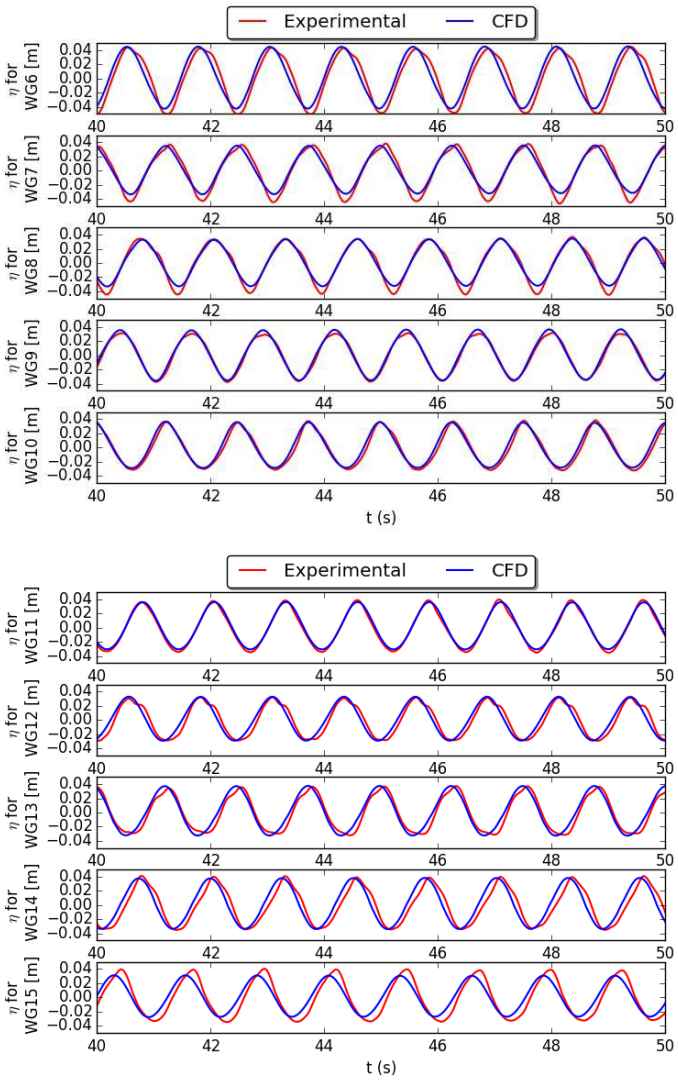

Fig. 14 Perturbed wave field using several wave gauges (see Fig. 2) around the 5WEC-array during a regular wave test (H = 0.074 m, T = 1.26 s, d = 0.70 m) obtained with CFD (blue line) compared to the experimental data (red line).

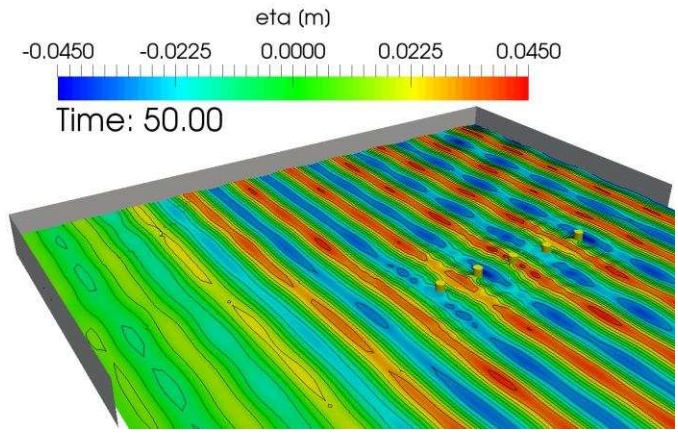

Fig. 15 A three dimensional snapshot of the perturbed wave field around the 5WEC-array during a regular wave test (H = 0.074 m, T = 1.26 s, d = 0.70 m) obtained with CFD.

V. Research Topics Under Investigation

The topics listed below will be investigated in the near feature:

- Simulations of a larger number of WECs arranged in various layouts (e.g. 3x3 array, 5x5 array, staggered arrays);
- Resonance simulations using regular waves with a period close to the WEC's natural period;
- Including turbulent effects in the numerical simulations;
- Simulating extreme storm conditions using focused waves which break on the array;
- Simulations of another WEC geometry (e.g. flat circular cylinder with a larger diameter to draft ratio).

VI. Conclusions

We have presented several cases of numerical simulations of two and five heaving WECs installed in a line array inside a numerical wave basin. Regarding the free decay test of the 2WEC-array on which the PTO system is activated, it was needed to include an additional linear damper apart from the PTO damper in order to take the influence of the supporting axis in the physical WEC into account. As a result, a fair agreement is obtained between numerical and experimental results. Not only the vertical position of the WECs and the surface elevations of the radiated wave field have shown a good agreement but also the surge force acting on the neighbouring WEC. Furthermore for the simulations of a 2WEC-array and a 5WEC-array subjected to a specific regular wave train, an additional coulomb damper has been implemented in order to include friction of the WEC with the supporting axis caused by the wave induced horizontal force. Those simulations also returned good results for its heave motion, the surge force on the WECs and the perturbed wave field around the WECs. However, some friction forces increasing the WEC's damping due to the presence of the supporting axis are still missing in the numerical model, producing deviating results. Those discrepancies are mainly observed in the WECs' heave motions and are rather limited in the surge forces acting on and the perturbed wave field around the WECs. In order to run simulations with more degrees of freedom (e.g. surge motion), a good prediction of the surge forces is required for example.

The numerical results have shown that our coupled CFD–motion solver is a robust and suitable toolbox to study wave-structure interaction. Moreover, it has been demonstrated that the coupled model is accurate to analyse the interaction between multiple WECs installed in an array configuration. In particular the WECs' heave motions, the surge force on the WECs and the perturbed wave field have been modelled very well. Moreover, the numerical model yields a much higher spatial resolution of the surface elevations in the numerical wave basin compared to the limited number of discrete measurements locations in the DHI wave basin. Future improvements will include numerical simulations of extreme storm events hitting the array to assess impact loads on the WECs and quantify the survivability of the array.

ACKNOWLEDGMENT

The first author is Ph.D. fellow of the Research Foundation – Flanders (FWO), Belgium (Ph.D. fellowship 1133817N).

The WECwakes project is funded by the EU FP7 HYDRALAB IV programme (contract no. 261520). The project is a consortium of seven European partners coordinated by Ghent University-Belgium (Peter Troch; Vasiliki Stratigaki). The construction of the WEC models at Ghent University (research grant FWO-KAN-15 23 712 N) and part of the data pre- and post-processing (Ph.D. funding grant of Vasiliki Stratigaki and research project no. FWO-3G029114), have been funded by the Research Foundation Flanders, Belgium (FWO).

REFERENCES

[1] K. Budal, "Theory for absorption of wave power by a system of interacting bodies," *J. Sh. Res.*, 1977.

[2] D. Evans, "Some analytic results for two and three dimensional wave-energy absorbers," *Power from sea waves*, 1980.

[3] J. Falnes, "Radiation impedance matrix and optimum power absorption for interacting oscillators in surface waves," *Appl. Ocean Res.*, 1980.

[4] "OpenFOAM®," *OpenFOAM-3.0.1*, 2015. [Online]. Available: http://www.openfoam.org/.

[5] B. Devolder, P. Rauwoens, and P. Troch, "Numerical simulation of a single Floating Point Absorber Wave Energy Converter using OpenFOAM®," in *Progress in Renewable Energies Offshore*, 2016, pp. 197–206.

[6] J. Davidson, M. Cathelain, L. Guillemet, T. Le Huec, and J. Ringwood, "Implementation of an OpenFOAM Numerical Wave Tank for Wave Energy Experiments," in *Proceedings of the 11th European wave and tidal energy conference*, 2015.

[7] H. A. Wolgamot and C. J. Fitzgerald, "Nonlinear hydrodynamic and real fluid effects on wave energy converters," *Proc. Inst. Mech. Eng. Part A J. Power Energy*, 2015.

[8] J. Davidson, S. Giorgi, and J. V. Ringwood, "Linear parametric hydrodynamic models for ocean wave energy converters identified from numerical wave tank experiments," *Ocean Eng.*, vol. 103, pp. 31–39, 2015.

[9] P. Stansby, H. Gu, E. C. Moreno, and T. Stallard, "Drag minimisation for high capture width with three float wave energy converter M4," in *11th European wave and tidal energy conference (EWTEC 2015)*, 2015.

[10] H. A. Wolgamot, P. H. Taylor, and R. Eatock Taylor, "The interaction factor and directionality in wave energy arrays," *Ocean Eng.*, vol. 47, pp. 65–73, 2012.

[11] A. Babarit, "On the park effect in arrays of oscillating wave energy converters," *Renew. Energy*, vol. 58, pp. 68–78, 2013.

[12] J. C. McNatt, V. Venugopal, and D. Forehand, "A novel method for deriving the diffraction transfer matrix and its application to multi-body interactions in water waves," *Ocean Eng.*, vol. 94, pp. 173–185, 2015.

[13] E. B. Agamloh, A. K. Wallace, and A. von Jouanne, "Application of fluid-structure interaction simulation of an ocean wave energy extraction device," *Renew. Energy*, vol. 33, no. 4, pp. 748–757, 2008.

[14] P. D. Mccallum, "Numerical methods for modelling the viscous effects on the interactions between multiple wave energy converters," PhD manuscript, The University of Edinburgh, 2017.

[15] B. Devolder, P. Rauwoens, and P. Troch, "Numerical simulation of heaving Floating Point Absorber Wave Energy Converters using OpenFOAM," in *VII International Conference on Computational Methods in Marine Engineering*, 2017.

[16] V. Stratigaki *et al.*, "Wave basin experiments with large wave energy converter arrays to study interactions between the converters and effects on other users in the sea and the coastal area," *Energies*, vol. 7, no. 2, pp. 701–734, 2014.

[17] C. W. Hirt and B. D. Nichols, "Volume of Fluid (VoF) Method for the Dynamics of Free Boundaries," *J. Comput. Phys.*, vol. 39, no. 1, pp. 201–225, 1981.

[18] B. Devolder, P. Rauwoens, and P. Troch, "Application of a buoyancy-modified k-ω SST turbulence model to simulate wave run-up around a monopile subjected to regular waves using OpenFOAM®," *Coast. Eng.*, vol. 125, pp. 81–94, Jul. 2017.

[19] B. van Leer, "Towards the ultimate conservative difference scheme. II. Monotonicity and conservation combined in a second-order scheme," *J. Comput. Phys.*, vol. 14, no. 4, pp. 361–370, 1974.

[20] P. Higuera, J. L. Lara, and I. J. Losada, "Realistic wave generation and active wave absorption for Navier-Stokes models. Application to OpenFOAM.," *Coast. Eng.*, vol. 71, pp. 102–118, 2013.

[21] P. Higuera, J. L. Lara, and I. J. Losada, "Simulating coastal engineering processes with OpenFOAM.," *Coast. Eng.*, vol. 71, pp. 119–134, 2013.

[22] B. Devolder, P. Schmitt, P. Rauwoens, B. Elsaesser, and P. Troch, "A Review of the Implicit Motion Solver Algorithm in OpenFOAM® to Simulate a Heaving Buoy," in *18th Numerical Towing Tank Symposium*, 2015.